Effect of Reactive Ball Milling Time on the Hydrogenation/Dehydrogenation Properties of Nanocomposite $MgH_2/7TiMn_{1.5}$ Powders

M. Sherif El-Eskandarany, H. Al-Matrouk, Ehab Shaban and Ahmed Al-Duweesh

Nanotechnology and Advanced Materials Program,
Energy and Building Research Center, Kuwait Institute for Scientific Research
Safat 13109, Kuwait - State of Kuwait, msherif@kisr.edu.kw

ABSTRACT

Nanocrystalline MgH_2 powders were prepared by high-energy reactive ball milling of pure Mg powders under 50 bar of a hydrogen gas atmosphere. The powders obtained after 200 h of milling were doped with 7 wt% of $Mn_{3.6}Ti_{2.4}$ powders and then ball milled 50 h, using a high energy ball mill. The as-milled $MgH_2/7Mn_{3.6}Ti_{2.4}$ nanocomposite powders obtained after 200 h of milling were homogeneous in shape (spherical-like), particle size (~ 1.5 μm in diameter) with grain size of less than 10 nm in diameter. (1.5 mm). This nanocomposite binary system enjoyed superior hydrogenation/dehydrogenation kinetics at 275°C, as elucidated by the short time required to absorb and desorb 5.3 wt% H_2 within 2 and 8 min, respectively. At this temperature the system possessed excellent absorption/desorption cyclability of 1000 complete cycles within 1400 h.

Keywords: reactive ball milling, metal hydrides, nanocatalysts, nanocomposites

1 INTRODUCTION

Since the beginning of 1990's reactive ball milling (RBM), which was introduced to the worldwide society of materials science and powder metallurgy by Calka [1] and El-Eskandarany et al. [2], has a well-known technique for preparing nanocrystalline metal hydrides and their composite powders [3]. However, MgH_2 has received a great attention as pioneering hydrogen storage material [4], the high thermal stability of MgH_2 system and its poor hydrogenation and consequence dehydrogenation kinetics, of it restric this attractive system to be utilized in real automobile applications. Mechanical alloying of MgH_2 with pure metal (e.g. Ti, Fe, Ni, Nb, V) [6], intermetallic compounds (e.g. $Zr_{100-x}Ni_x$ alloys) [7] and dual metal/metal oxide composite (e.g. Ni/Nb_2O_5) [8] powders is considered as a promising approach used for enhancing the hydrogenation/dehydrogenation kinetics of MgH_2.

The present study has been addressed in part to investigate the effect of ball milling time on developing homogeneous nanocomposite MgH_2/7wt% $TiMn_{1.5}$ powder particles with uniform composition and micro/nano-structures. In addition, the effect of grain/particle distributions of $TiMn_2$ additive on improving the hydrogenation/dehydrogenation kinetics of MgH_2 powder matrix were investigated in terms of structure, morphology, thermal stability, hydrogen storage capacity and cyclability.

2 EXPERIMENTAL PROCEDURE

Pure Mg metal powders (~ 80 μm, 99.8 %), $TiMn_{1.5}$ shots (~ 800 μm, 99.8 %) and hydrogen gas (99.999 %) were used as starting materials. A certain amount of the Mg powders (5 g) was balanced inside a helium (He) gas atmosphere (99.99%) - glove box and then were sealed together with twenty five hardened steel balls into a hardened steel vial (220 ml in volume), using a gas-temperature-monitoring system (GST). The ball-to-powder weight ratio was 40:1. The vial was then evacuated to the level of 10^{-3} bar before introducing H_2 gas to fill the vial with a pressure of 50 bar. The milling process was carried out at room temperature using high energy ball mill operated at a rotation speed of 250 rpm. After 200 h of RBM the powders were discharged from the vial inside the glove box and sealed into Pyrex vails. The as-synthesized MgH_2 powders were then mixed in the glove with 7 wt.% $TiMn_{1.5}$ shots, using an agate mortar and pestle. Five gram of the mixed powders for each composite system were charged together with twenty five hardened steel balls into the hardened steel vial and sealed under He gas atmosphere. The vial was then filled with 50 bar of hydrogen gas atmosphere and mounted on the high energy ball mill. The milling process was interrupted after selected time (3, 6, 12.5, 25, 37.5 and 50 h) to get a small amount of the milled powders.

The powders were then characterized by means of X-ray diffraction (XRD) with CuKα radiation, 200 kV-field emission high resolution transmission electron microscopy/scanning transmission electron microscopy (FE-HRTEM/STEM), equipped with energy-dispersive X-ray spectroscopy (EDS), 15 kV-field emission scanning electron microscope (FE-SEM/EDS). The hydrogenation properties; including the pressure-composition-temperature (PCT) and absorption/desorption kinetics were investigated via Sievert's method.

The thermal stability of the ball milled powders indexed by the decomposition temperature of MgH_2 and activation energy, for the nanocomposite powders were investigated by means of a differential scanning calorimeter (DSC) at different heating rate.

3 RESULTS AND DISCUSSIONS

Figure 1 shows the XRD patterns of nanocomposite MgH_2/7 $Mn_{3.5}Ti_{2.4}$ powders obtained after selected ball milling time. The starting material powders (0 h) consisted of nanocrystalline MgH_2 powders with broad Bragg reflections of β- and γ- phases coexisted with sharp Bragg reflections of micrograined hcp-$Mn_{3.5}Ti_{2.4}$ powders, as shown in Fig. 1(a). During the early stage of ball milling (6 to 12.5 h), the Bragg peaks corresponding to hcp-$Mn_{3.5}Ti_{2.4}$ showed considerable broadening, implying the achievement of size reduction grain refining and the formation of finer hcp-$Mn_{3.5}Ti_{2.4}$ crystallites, as shown in Figs. 1(b) and 1(c). Further ball milling time (25 to 37.5 h) leads to further broadening on the Bragg peaks corresponding to hcp-$Mn_{3.5}Ti_{2.4}$ phase, as presented in Figs. 1(d) and 1(e). This obvious broadening suggests the continuity of the plastic deformation assisted by the milling media. Further broadening associated with a remarkable decreasing in the intensity of the Bragg peaks related to hcp-$Mn_{3.5}Ti_{2.4}$ phase is obviously seen upon ball milling for 50 h (Fig. 1(f)), indicating the formation of nanophase hcp-$Mn_{3.5}Ti_{2.4}$ powder coexisted with nanograined of MgH_2 powders.

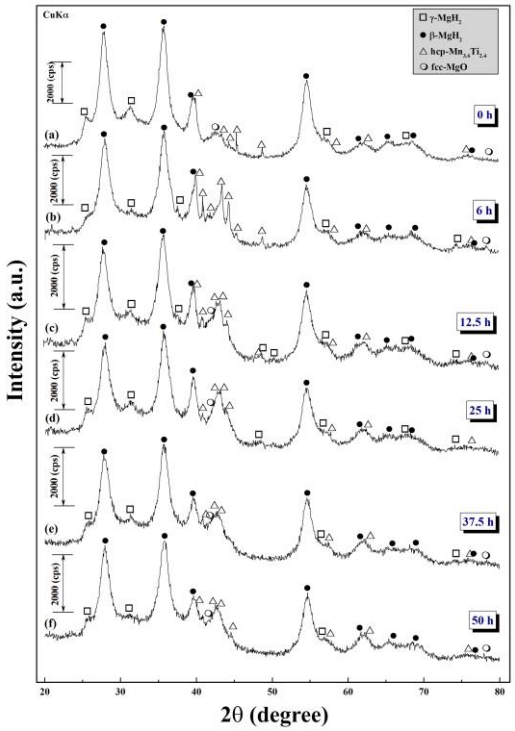

Figure 1: XRD patterns of MgH_2 powders obtained after 200 h of RBM and then ball milled with 7 wt% $Mn_{3.6}Ti_{2.4}$ powders under 50 bar of a hydrogen gas atmosphere for (a) 0, (b) 6, (c) 12.5, (d) 25, (e) 37.5, and (f) 50 h.

The HRTEM image of the powders after the final stage of ball milling (50 h) is shown in Fig. 2. The image showing atomic facets of two individual $Mn_{3.6}Ti_{2.4}$ nanocrystals (~ 7 nm in diameter) oriented to [103] and [110]. These nanocrystals were embedded into the MgH_2 matrix, indexed by the Moiré-like fringes corresponding to β- and γ-phases (Fig. 2). In the figure, the metallic $Mn_{3.6}Ti_{2.4}$ nanoscaled grains formed high misorientation angle phase boundaries at the interfaces of MgH_2 grains. At this atomic TEM resolution, neither different hydride phase(s) rather than MgH_2 nor intermediate reacted phase(s) could be detected in the MgH_2 matrix or at the grain boundaries of MgH_2/$Mn_{3.6}Ti_{2.4}$ interfaces, suggesting the formation of binary nanocomposite MgH_2/$Mn_{3.6}Ti_{2.4}$ system. Based on careful TEM investigations performed in the present study for at least 40 tested zones of six different individual samples, we could not detect any other phases rather than the starting materials of MgH_2 and $Mn_{3.6}Ti_{2.4}$. It is worth mentioning that no intermediate phase (reacted phase) could be detected even after ball milling for 50 h and the end-product at this stage of milling consisted of two individual distinguished phases of MgH_2 matrix powders doped with nanocrystallite $Mn_{3.5}Ti_{2.4}$ grains. Moreover, the crystal structure of the starting materials of $Mn_{3.5}Ti_{2.4}$ did not change upon increasing the ball milling time.

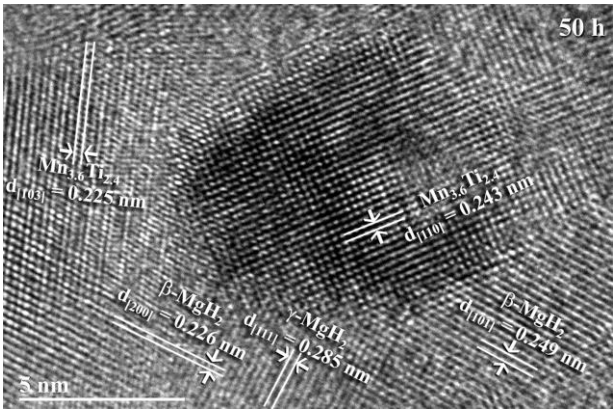

Figure 2: HRTEM image of the nanocomposite powders obtained after 50 h of the ball milling time.

In order to get more information about the effect of ball milling time on the distribution of $Mn_{3.6}Ti_{2.4}$ powder particles embedded into the host MgH_2 matrix; intensive STEM-EDS X-ray elemental mapping were performed for all the samples after ball milling time. Figure 3 presents the STEM-BF images (a, e, and i) and the corresponding EDS chemical mapping for Mg (b, f, and j), Ti (b, g, and k) and Mn (d, h, and l) for three selected samples obtained after 3 h (a-d), 12.5 h (e-h) and 50 h (i-l) of the ball milling time. The MgH_2/$Mn_{3.6}Ti_{2.4}$ composite powders obtained after 3 h of ball milling consisted of fine MgH_2 matrix (Figs. 3(a) and 3(b)) doped with large thick bulk particles (dark zones shown in Fig. 3(a)) of $Mn_{3.6}Ti_{2.4}$ (Figs. 3(c) and 3(d)). At this stage of milling, the local composition of the composite powders was widely varied from particle to particle and within the particle in both nano- and micro- levels. The local chemical analysis of $Mn_{3.6}Ti_{2.4}$ concentration

measured with an average area of 2 μm was in the range between 0 to 74 wt%. These $Mn_{3.6}Ti_{2.4}$ large powder particles tended to lose their original flake-like morphology upon increasing the ball milling time to 12.5 h and forming finer cells with large size distribution ranging from 70 to 200 nm in diameter (Fig. 3(e)) existed in the MgH_2 matrix (Fig. 3(f)). At this stage of ball milling, the $Mn_{3.6}Ti_{2.4}$ particles were heterogeneously embedded into the of the MgH_2 matrix and concentrated mainly near the edge of powder matrix, as shown in Figs. 3(g) and 3(h). Whereas the average $Mn_{3.6}Ti_{2.4}$ concentration at the near-edge composite powders was about 5 wt%, the concentration of this phase was less than 2 to 3.8 wt% in the core of the MgH_2 matrix. Toward the end of the ball milling processing time (50 h), the powders were aggregated to form heart-like morphology particles with an apparent particle size of about 250 nm in diameter (Fig. 3(i)). These aggregated particles consisted of MgH_2 (matrix) doped with nano-sized $Mn_{3.6}Ti_{2.4}$ dispersoids (Figs. 3(j), 3(k), and 3(l)). At this final stage of ball milling, the $Mn_{3.6}Ti_{2.4}$ particles possessed lens-like morphology with particle size distribution laying in the range between 8 nm to 32 nm in diameter, as displayed in Figs. 3(k) and 3(l). It is worth notifying that the $Mn_{3.6}Ti_{2.4}$ nano-cells were homogeneously distributed in the MgH_2 matrix to form uniform nanocomposite $MgH_2/Mn_{3.6}Ti_{2.4}$ with an average composition ranged from 6.7 to 7.4 wt% in all the examined zones (36 ones) for 8 individual nanocomposite samples.

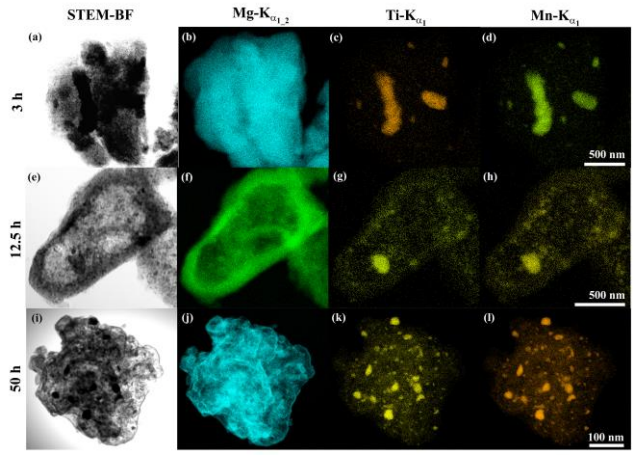

Figure 3: STEM-BF micrographs and the corresponding X-ray elemental mapping of MgH_2/7 $Mn_{3.6}Ti_{2.4}$ powders obtained after 3 h (a-d), 12.5 h (e-h), and 50 h (i-l) of the ball milling time.

The absorption and desorption kinetics performed at 275ºC for nanocomposite MgH_2/7 wt% $Mn_{3.6}Ti_{2.4}$ powders obtained after different ball milling time are shown in Fig. 4(a) and 4(c), respectively. The shaded area indexed in Figs. 4(a) and 4(c) are shown in different scale in Fig. 4(b) and 4(d), respectively. The starting materials at 0 h ball milling (hand-mixed powders) absorbed 2.66 wt% H_2 within 1 min, as shown in Fig. 4(b). The hydrogen absorbed content of this sample is increased monotonically with increasing the absorption time to be saturated at about 5.5 wt% after 13 min, as shown in Fig. 4(a). Increasing the ball milling time (3 – 25 h) led to decrease the time required for absorption, exemplified by the sample obtained after 25 h in which 1 min was enough to absorb 3.89 wt% H_2, as shown in Fig. 4(b). The hydrogen concentration of this sample reached to a saturated value of about 5.2 wt% after 4.5 min, as shown in Fig. 4(a). After 37.5 h of the ball milling time, the powder possessed faster absorption kinetics indexed by increasing the absorbed amount of hydrogen (4.5 wt%) performed at 1 min, as displayed in Fig. 4(b). The hydrogen concentration of this sample showed a saturation value of about reached to a saturated value of about 5.1 wt% after 3.6 min, as shown in Fig. 4(a). The powders of the end-product (50 h) shows superior absorption kinetics, characterized by the very short absorption time (1 min) required to absorb 5 wt% H_2, as shown in Fig. 4(b). This value reached to about 5.3 wt% after 2 min and it did not show any changes even after 12 min of the hydrogen absorption time, as elucidated in Fig. 4(a).

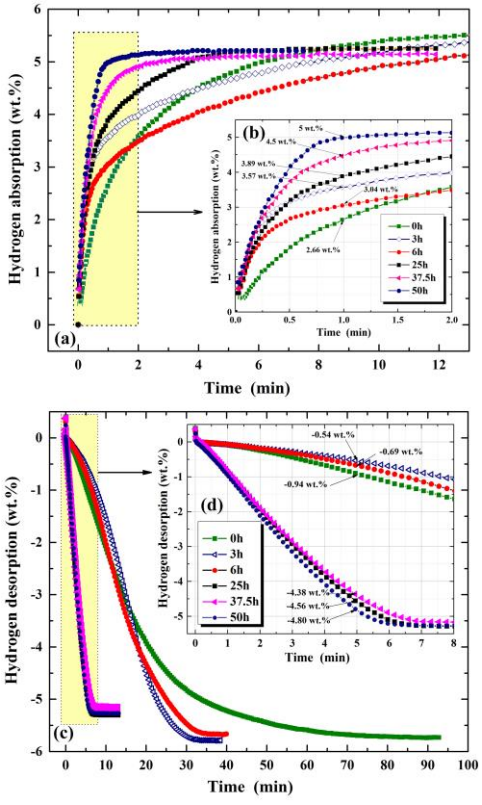

Figure 4: Effect of ball milling time on the (a) hydrogenation and (b) dehydrogenation kinetics of nanocomposite MgH_2/7 wt% $Mn_{3.6}Ti_{2.4}$ powders.

The kinetics of dehydrogenation for the powders at the early stage of ball milling time (0 – 6 h) were very slow, suggested by the low H_2 content (-0.54 to -0.94 wt%) after

5 min of the desorption time (Fig. 4(d)). A full dehydrogenation process was achieved on the samples at this early stage of ball milling for releasing H_2 content in the range between 5.6 – 5.8 wt% with a duration of time ranging between 35 min to 85 min, as shown in Fig. 4(c). In contrast to those samples of the early stage, the powders obtained after 25 h (intermediate stage) and 37.5 h (final stage) of ball milling possessed excellent desorption kinetics, indicated by the short time required (5 min) to release about -4.38 to -4.56 wt% H_2 (Fig. 4(d)). The value of released H_2 content tended to be saturated at about 5.3 wt%H_2 after 6.8 min, as shown in Fig. (Fig. 4(d)). No remarkable improvement in the hydrogen desorption kinetics could be notified for the sample obtained after 50 h of the ball milling time. It just shows a little increasing in the content of H_2 (~ -4.8 wt%) released after 5 min of the desorption time and saturated at 5.3 wt% after about 6.8 min, as shown in Fig. 4(d). Increasing the hydrogen absorption processing time to 14 min did not lead to obvious improvement on the amount of H_2 released, as shown in Fig. 4(c).

The cycle-life-time conducted at 275ºC for nanocomposite MgH_2/7 wt% $Mn_{3.6}Ti_{2.4}$ powders obtained after 50 h of ball milling time is shown in Fig. 5. This binary system possessed an excellent hydrogenation/dehydrogenation cyclability, demonstrated by achieving continuous 1000 cycles within 1400 h without failure (Fig. 5). During the first 410 h of cycle-life-time, the fabricated nanocomposite powders maintained their fast kinetics fashion of up-taking and releasing an amount of 5.3 wt% H_2 within 2 min and 5 min respectively, as shown in Fig. 5. A minor degradation in the hydrogen storage capacity and the kinetics of hydrogenation/dehydrogenation occurred upon increasing the cycle-life-time from 410 h to 1400 h. This slight degradation took place as a result of the grain growth came off in the Mg/$Mn_{3.6}Ti_{2.4}$ powder particles, as suggested by HRTEM analysis (Fig. 6).

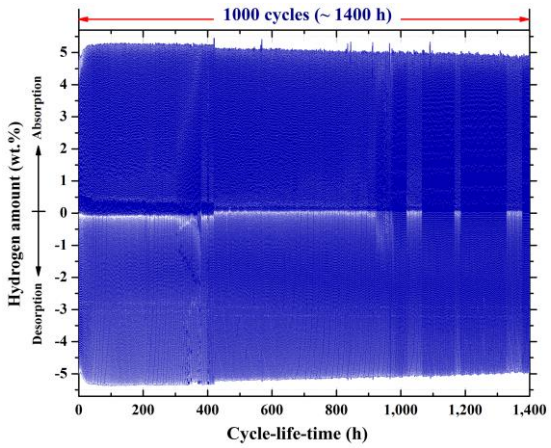

Figure 5: Hydrogenation/dehydrogenation curves of 1000 complete cycles conducted at 275 ºC for MgH_2/7 $Mn_{3.6}Ti_{2.4}$ nanocomposite powders obtained after 50 h of the ball milling time.

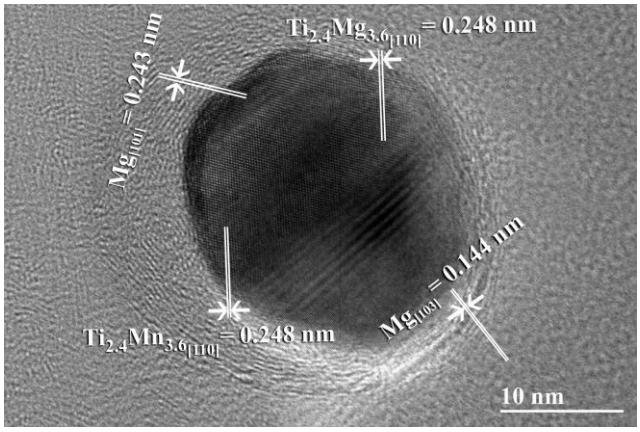

Figure 6: HRTEM images of a typical MgH_2/7 $Mn_{3.6}Ti_{2.4}$ nanocomposite particle obtained after 50 h of the ball milling time and then subjected to 1000 continuous hydrogen-absorption/desorption cycles at 275 ºC.

4 CONCLUSIONS

Mechanical ball milling technique, using a high energy ball mill was employed to prepare MgH_2/7 $Mn_{3.6}Ti_{2.4}$ nanocomposite powders. This nanocomposite binary system enjoyed superior hydrogenation/dehydrogenation kinetics at 275ºC, as elucidated by the short time required to absorb and desorb 5.3 wt% H_2 within 2 and 8 min, respectively. At this temperature the synthesized nanocomposite powders possessed excellent absorption/desorption cyclability of 1000 complete cycles within 1400 h..

REFERENCES

[1] A. Calka, Appl. Phys. Lett., 59, 1568-1570, 1991.

[2] M. Sherif El-Eskandarany, K. Sumiyama, K. Aoki, and K. Suzuki, Mater. Sci. Forum, 88, 801-808, 1992.

[3] Robert A Varin, Tomasz Czujko, and Zbigniew S.Wronski, "Nanomaterials for Solid State Hydrogen Storage. 1st ed., Springer Science+Business Media, LLC 2009.

[4] M Sherif El-Eskandarany, "Mechanical Alloying for Nanotechnology, Materials Science and Powder Metallurgy," 2nd ed., Elsevier Publishing, Oxford-UK, 2015, in press.

[5] M. Sherif El-Eskandarany, Ehab Shaban, and Badryiah Al-Halaili, Int. J. Hydrogen Energy, 39, 12727-12740, 2014.

[6] C.X. Shang, M. Bououdina, Y. Song, Z.X. Guo, Int. J. Hydrogen Energy, 29, 73-80, 2004.

[7] B. Molinas, A.A. Ghilarducci, M. Melnichuk, H.L. Corso, H.A. Peretti, F. Agresti, A. Bianchin, Russo S. Lo, A. Maddalena and G. Principi, Int. J. Hydrogen Energy, 34, 4597-4601, 2009.

[8] M. Sherif El-Eskandarany, Ehab Shaban, Ahmed Al-Shemmiri, Int J Hydrogen Energy, 39, 21097-21106, 2014.